SUPPORTING INFORMATION

Why GPCRs behave differently in cubic and lamellar lipidic mesophases

George Khelashvili[1], Pedro Blecua Carrillo Albornoz[1], Niklaus Johner[1], Sayan Mondal[1], Martin Caffrey[3], Harel Weinstein[1,2]

[1]Weill Cornell Medical College of Cornell University, New York, NY, 10065

[2]The HRH Prince Alwaleed Bin Talal Bin Abdulaziz Alsaud Institute for Computational Biomedicine, Weill Cornell Medical College, Cornell University, New York, NY 10065

[3]Membrane Structural and Functional Biology Group, School of Biochemistry and Immunology, and School of Medicine, Trinity College, Dublin

Supporting Methods

Coarse-grained parameters for 9.9 MAG lipid

The parameterization of 9.9 MAG compatible with the CG Martini lipid force-field version 2.0 was achieved by dividing the 9.9 MAG all-atom structure into 7 standard coarse-grained beads (Fig. 1A): one bead for the headgroup (ETH), one for the ester linkage (GL1), and 5 beads for the hydrocarbon tail (C1A, C2A, D3A, C4A, C5A) [1]. For the glycerol and the 5 tail beads, the Martini types were set, respectively, to the standard "Na" type, and the "C1-C1-C3-C1-C1" sequence of bead types [1]. The headgroup ETH bead was designated as "P4" type, similar to that found in the Martini parameter set for 1,2-dioleoyl-*sn*-glycero-3-phospho-(1'-*rac*-glycerol) (DOPG) lipid [2] which also possesses an OH-C-C-OH headgroup (Fig. 1A). However, for 9.9 MAG, the ETH bead/water LJ interaction parameter was increased here from 5.0 to 5.6 kJ/mol [3] in order to take into account the special properties of 9.9 MAG, as described below. The parameterization of the bonded interactions was performed following the standard set of bonded parameters for lipids in the Martini version 2.0 [1] with a single exception: the equilibrium angle for the GL1-C1A-C2A triplet was set to 140^0 (instead of the default value of 180^0). The special structure of 9.9 MAG made it necessary to introduce the two adjustments described above, implemented equally in both the cubic and the lamellar phase simulations, in order to account for the different curvature propensity expected of a single-tail 9.9 MAG compared to the double-tail phospholipids, such as DOPG.

The set of CG force-field parameters was tested first on lamellar bilayers formed by 9.9 MAG, in simulations of membranes containing 472 9.9 MAG lipids and 15104 water molecules. These simulations, conducted at 27^0C for 40ns under semi-isotropic pressure coupling conditions and with a 40fs time step, yielded structural characteristics of the 9.9 MAG bilayer in good agreement with those reported from all-atom MD simulations [4], as well as from experimental measurements on 9.9 MAG [38,39]. Specifically, in our CG simulations we found the area per 9.9 MAG head-group to be 37.5□0.5 Å^2, a value similar to experimentally measured 37.9 Å^2 [4]. Furthermore, the calculated thickness of the 9.9 MAG bilayer (measured from the peak-to-peak distance on the density plot of ETH/GL1 pair of beads) was 34.7□1 Å, consistent with the 33-37 Å range for the bilayer thickness (depending on the extent of

solvation) reported from X-ray diffraction experiments [5] and all-atom MD simulations [4]. In addition, measured from the peak-to-peak distance on the density plot of the D3A double bond bead, the average separation between the C9=C10 unsaturated bonds on the two leaflets of the bilayer is 12.8□1 Å, in good agreement with results from atomistic MD simulations [4]. The close match between the structural properties of CG 9.9 MAG bilayer obtained from our CG simulations and those obtained experimentally or with all-atom MD simulations supports the CG parametrization we developed for the exploration of the cubic phases formed by 9.9 MAG.

Coarse-grained representation of rhodopsin

The structure of rhodopsin was obtained from PBD 1U19, represented at the CG level as described before [6], and using the recent 2.1 version of the Martini force-field [7]. Similar to the protocols used in earlier CG studies of rhodopsin [6]: 1)-the protein secondary structure elements were maintained unchanged throughout the CG simulations through appropriate bond interaction parameters; 2)-the disulfide bridge between C110 and C187 was introduced in the force-field through covalent bonding; 3)-the protonated forms of Asp83, Glu122, and Glu181 in the CG model were represented by Asp and Glu by Asn and Gln, respectively; and 4)-palmitoyl chains were not included in the CG model.

References

(1) Marrink, S. J.; Risselada, H. J.; Yefimov, S.; Tieleman, D. P.; de Vries, A. H. *J Phys Chem B* **2007**, *111*, 7812-24.

(2) Baoukina, S.; Monticelli, L.; Risselada, H. J.; Marrink, S. J.; Tieleman, D. P. *Proc Natl Acad Sci U S A* **2008**, *105*, 10803-8.

(3) Marrink, S. J.; Mark, A. E. *Biophys J* **2004**, *87*, 3894-900.

(4) Wilson, M. A.; Pohorille, A. *J Am Chem Soc* **1994**, *116*, 1490-501.

(5) Pezron, I.; Pezron, E.; Bergenstahl, B. A.; Claesson, P. M. *Journal of Physical Chemistry* **1990**, *94*, 8255-8261.

(6) Periole, X.; Huber, T.; Marrink, S. J.; Sakmar, T. P. *J Am Chem Soc* **2007**, *129*, 10126-32.

(7) Monticelli, L.; Kandasamy, S. K.; Periole, X.; Larson, R. G.; Tieleman, D. P.; Marrink, S. J. *Journal of Chemical Theory and Computation* **2008**, *4*, 819–834.

Figure Legends

Figure S1: Two views of Rhodopsin (in *yellow*) inserted randomly in the lipid cubic phase for the start of the simulation. The lipid system as shown was obtained by magnifying 27 times (i.e., 3 times in positive and negative *x, y,* and *z* directions) the last snapshot from the 9.9 MAG/water complex simulation (Figure 2 of the main text). The cubic phase is shown by depicting water beads (cyan) and the 9.9 MAG lipid headgroup beads (*pink*).

Figure S2: TPMS approximation to the cubic phase of *Pn3m* symmetry (*continuous analytical surface)* constructed using Eqs. (1-3). The locations of the C5A beads (in *green*) from the simulations of 9.9 MAG/water complex at 40 % w/w water and 20^0C are obtained from the alignment of 20 trajectory frames using a fitting procedure described in Methods.

Figure S3: Views of the 9.9 MAG/water system from simulations at 40 % (w/w) water concentration and 20^0C temperature (see Table 1 of the main text), after independent 6 μs of self-assembly simulations (the third simulation at 40 % (w/w) water and at 20^0C is discussed in detail in the main text). For each simulated system, panels *A* and *B* show the organization of 9.9 MAG head-group and water beads, respectively, in representations of the of the simulation unit cell magnified 27 times (i.e., 3 times in positive and negative *x, y,* and *z* directions). Panels *C-E* offer various views of the two non-intersecting continuous water channels (shown in cyan and gold colors) in the respective simulations. Panels *F* in each Figure show the distributions of $\{C_i\}$ coefficients as derived from the fitting of the simulated structures to the TPMS of the *Pn3m* phase (the standard deviation of each distribution is ~0.4). The χ^2 test established the significance of the fit with probability $p<0.05$.

Figure S4: Views of Rhodopsin TMH1 and TMH5 helices (in *yellow*) equilibrated in the lamellar mesophase showing the mismatched positions of residues Pro34$^{1.29}$ (in *red*), Gln36$^{1.31}$ (*green*), and Phe228$^{5.63}$ (*blue*). The lipid environment is represented by the location of 9.9 MAG lipid hydrophobic core beads (*in purple*). The snapshots were generated from the last frame of a 3.2 μs-long MD trajectory.

Figure S5: Classification of rhodopsin residues according to their proximity to the LCP region that is most perturbed from the *Pn3m* organization (according to the *S* score defined in Eq. (5) in the

Main text). The residues that contact the lipid bilayer where it is most deformed from the diamond cubic phase, are shown as blue spheres; the rest of the protein is depicted as red spheres. The lipid bilayer within 25Å of the protein is represented by the location of the C1A 9.9 MAG lipid backbone beads (*gray spheres*). Residues Pro34$^{1.29}$ and Phe228$^{5.63}$ are highlighted in yellow.

Figure S6: : Identification of contact interfaces in the crystal structures of various GPCRs obtained from *in meso* crystallization. The 12 rhodopsin-like GPCRs used in this analysis are: β_2 adrenergic receptor – PBD codes: 2RH1, 3PDS, 3SN6; A2A receptor – PDB codes: 3EML, 3QAK; Chemokine CXCR4 receptor – PDB codes: 3ODU, 3OE0, 3OE6, 3OE8, 3OE9; Dopamine D3 receptor – PDB code: 3PBL, and Histamine H1 receptor – PDB code: 3RZE). Only interfaces where the crystallographic contacts were formed exclusively through inter-monomer TM-TM interactions were considered. (*A*) Shows the fraction of GPCR structures that have at least one specific TM-TM contact interface (*red bars*), and the average number of contacts between TM pairs throughout the structural library (*blue bars*). (*B*) Shows the fraction of GPCR structures that have specific residue on TMH1 at least once at the contact interface throughout the structural library (*red bars*), and the average number of contacts particular residue on TMH1 makes throughout the structural library (*blue bars*). (*C*) Same as in panel *B* only for TMH5 residues. Residue numbering in panels *B-C* are given in Ballesteros & Weinstein numbering.

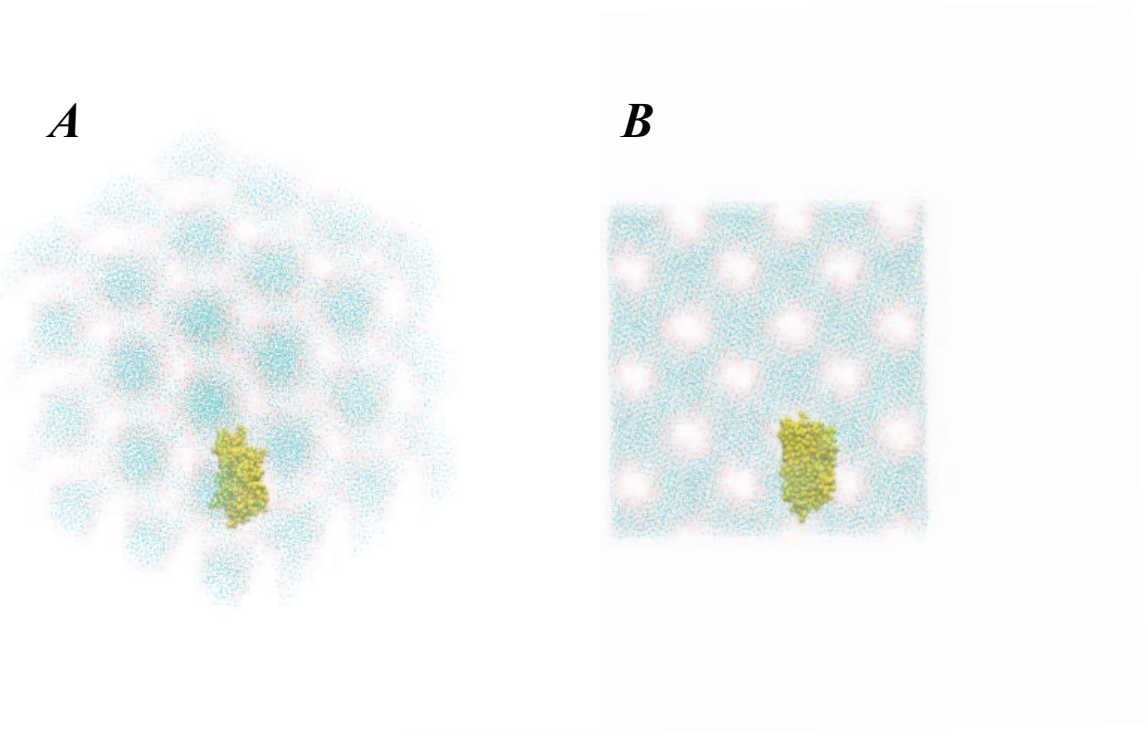

Figure S1

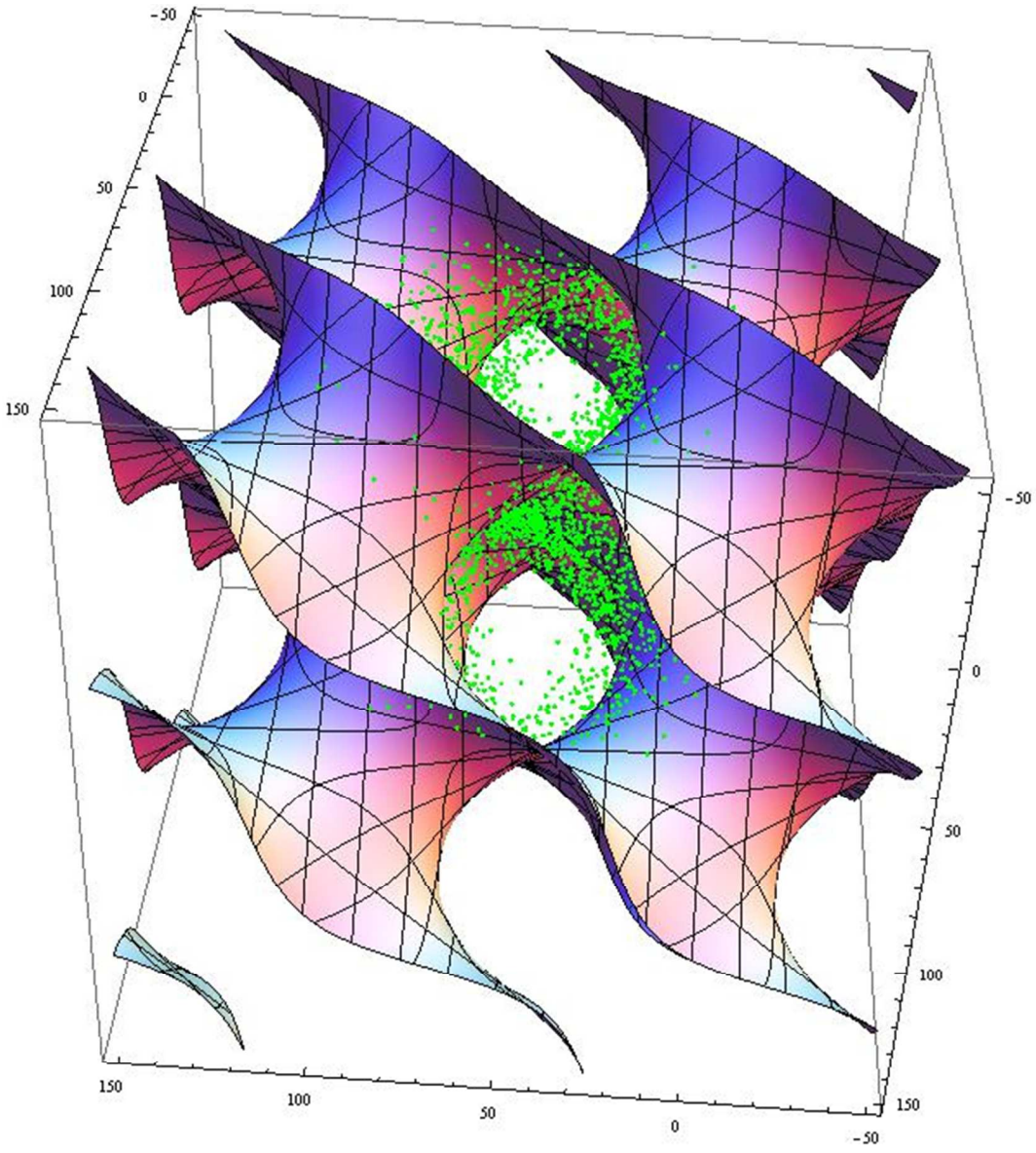

Figure S2

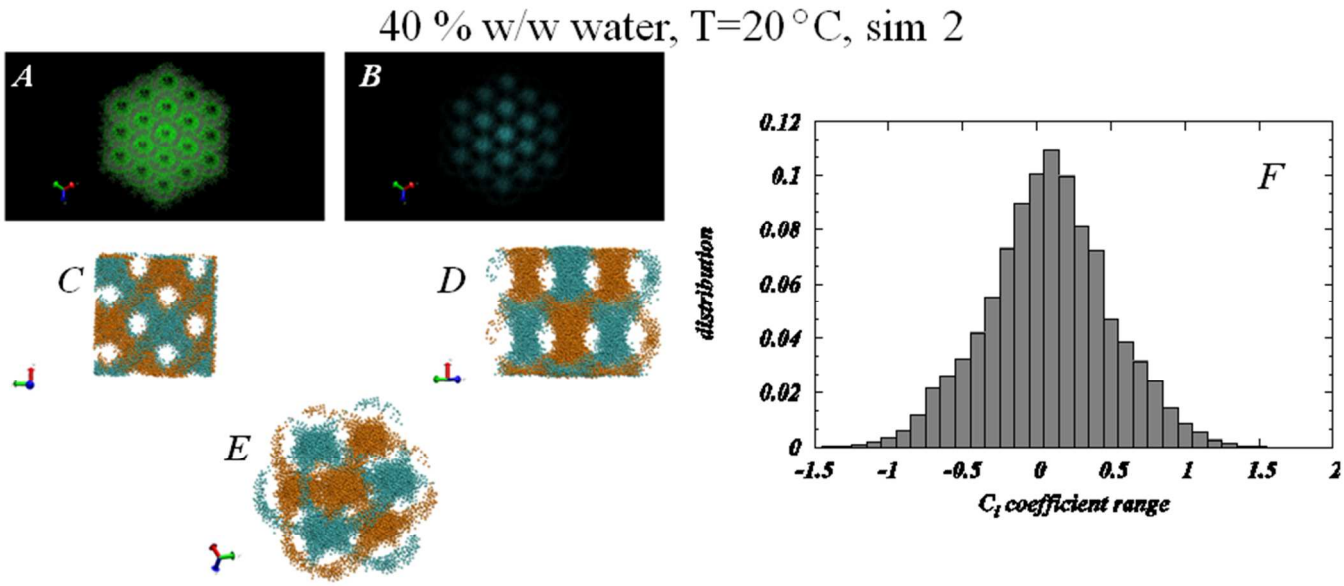
40 % w/w water, T=20 °C, sim 2
A
B
C
D
E
F
distribution
0.12
0.1
0.08
0.06
0.04
0.02
0
-1.5
-1
-0.5
0
0.5
1
1.5
2
C_i coefficient range

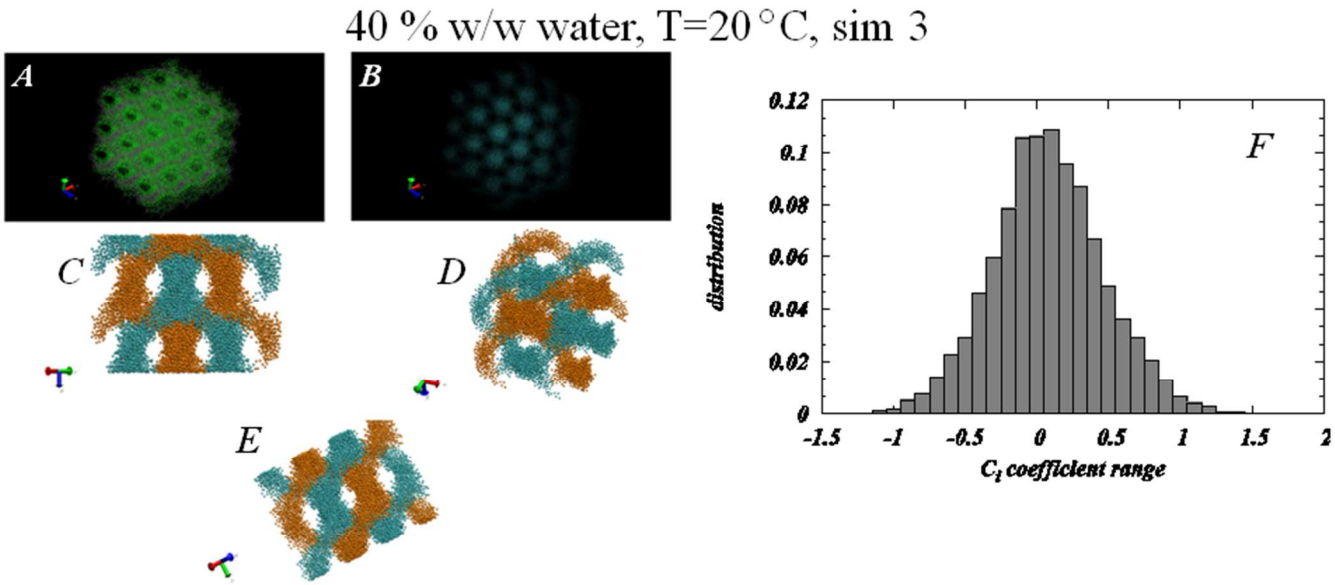
40 % w/w water, T=20 °C, sim 3
A
B
C
D
E
F
distribution
0.12
0.1
0.08
0.06
0.04
0.02
0
-1.5
-1
-0.5
0
0.5
1
1.5
2
C_i coefficient range

Figure S3

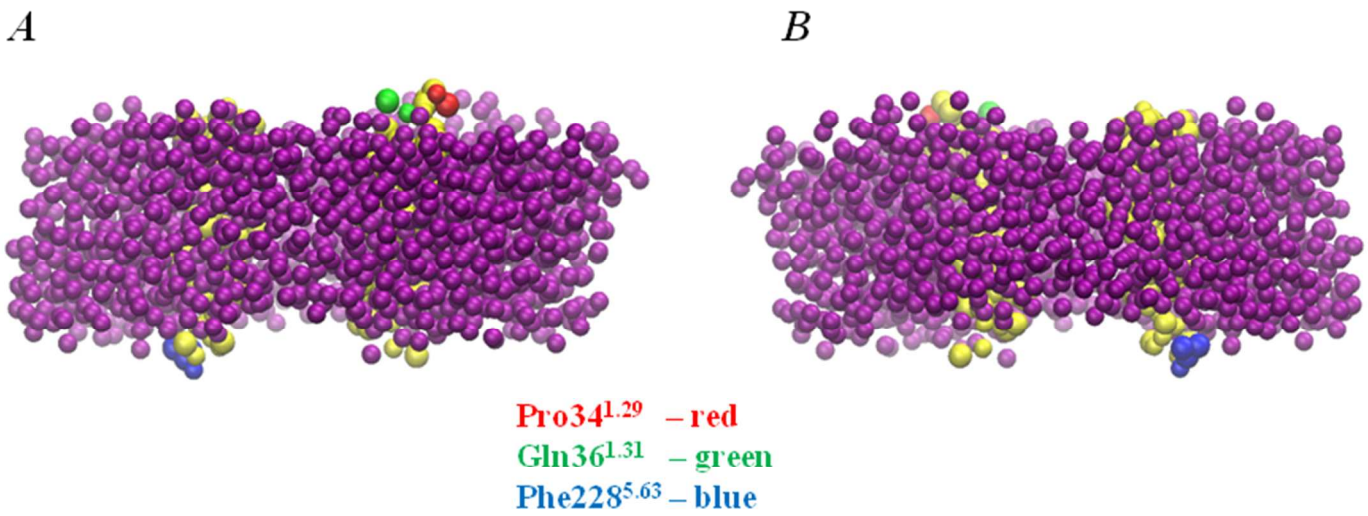

Figure S4

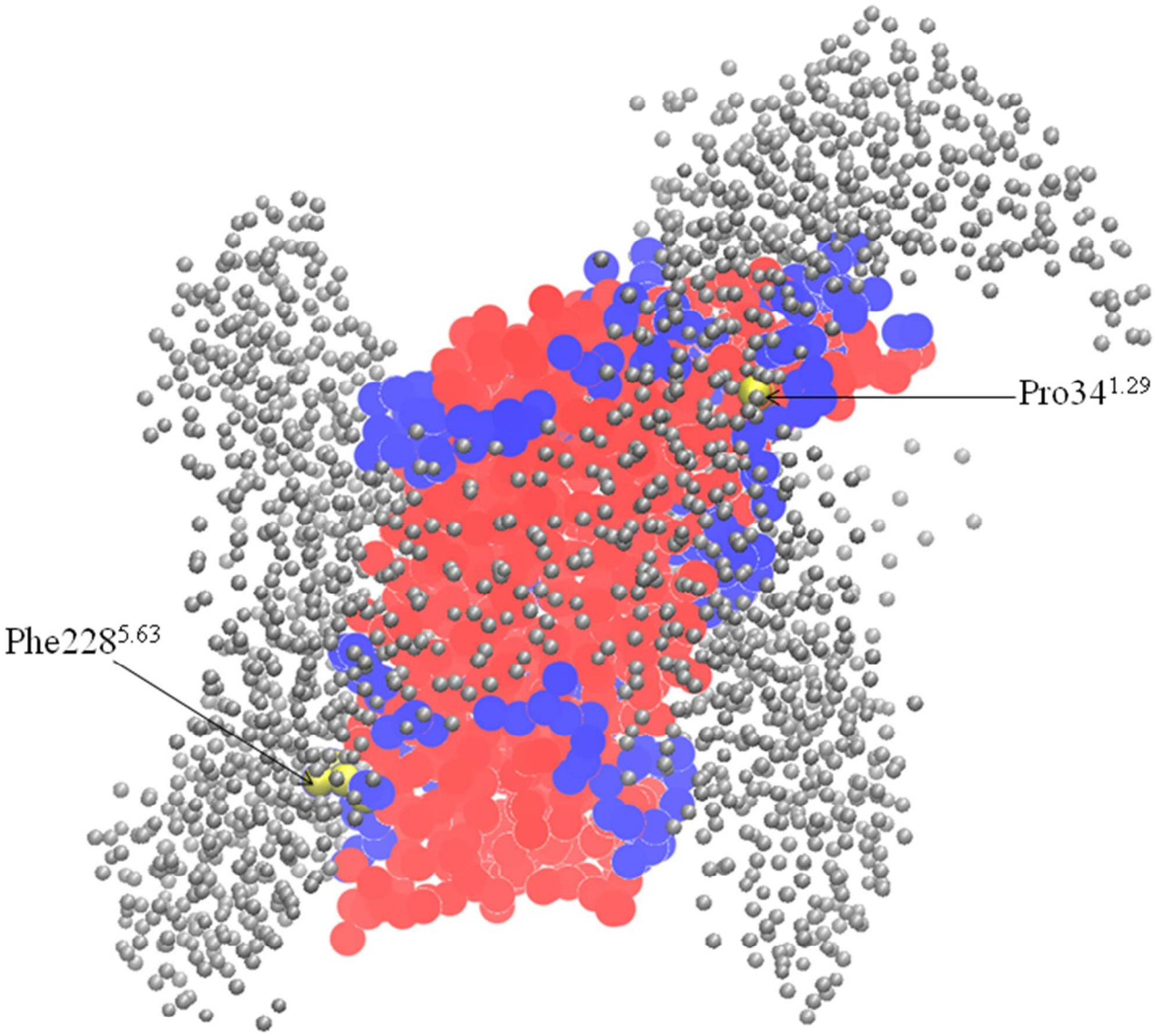

Figure S5

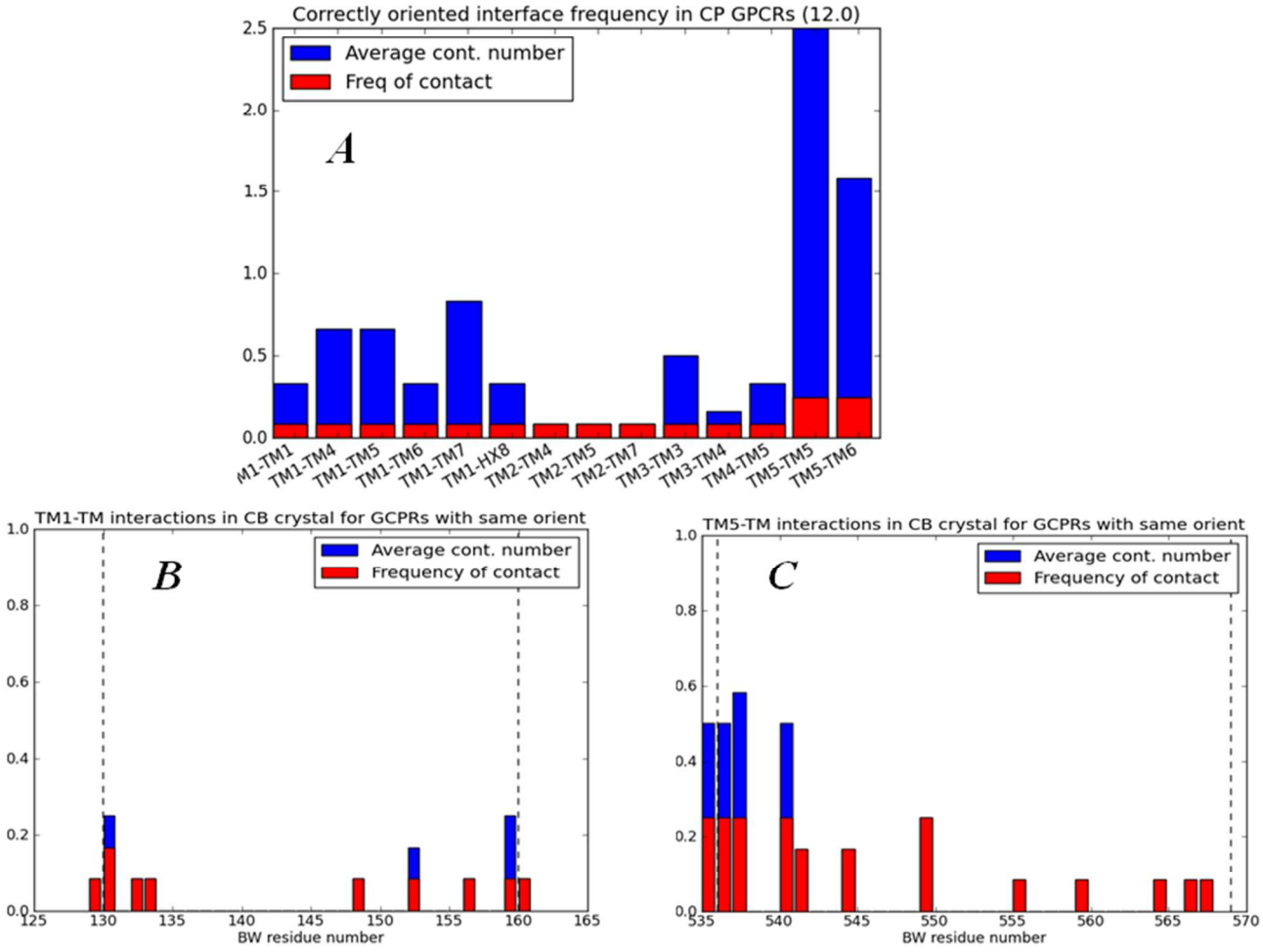
Correctly oriented interface frequency in CP GPCRs (12.0)
Average cont. number
Freq of contact
A
2.5
2.0
1.5
1.0
0.5
0.0
M1-TM1
TM1-TM4
TM1-TM5
TM1-TM6
TM1-TM7
TM1-HX8
TM2-TM4
TM2-TM5
TM2-TM7
TM3-TM3
TM3-TM4
TM4-TM5
TM5-TM5
TM5-TM6
TM1-TM interactions in CB crystal for GCPRs with same orient
Average cont. number
Frequency of contact
B
1.0
0.8
0.6
0.4
0.2
0.0
125
130
135
140
145
150
155
160
165
BW residue number
TM5-TM interactions in CB crystal for GCPRs with same orient
Average cont. number
Frequency of contact
C
1.0
0.8
0.6
0.4
0.2
0.0
535
540
545
550
555
560
565
570
BW residue number

Figure S6